10148 *Inorg. Chem.* **2010**, *49*, 10148–10155
DOI: 10.1021/ic1016033

Inorganic Chemistry
Article

Ternary Nitride $GaFe_3N$: An Experimental and Quantum-Theoretical Study

Jens Burghaus, Michael Wessel, Andreas Houben, and Richard Dronskowski*

Institut für Anorganische Chemie, RWTH Aachen University, Landoltweg 1, 52056 Aachen, Germany

Received August 8, 2010

The recently published two-step ammonolysis reaction giving access to phase-pure $GaFe_3N$ has been reinvestigated. Thermochemical calculations show that a high-temperature route is necessary to avoid the formation of the competing GaN phase. Compared to the prior study showing a Vegard-like behavior (that is, a linear correlation between lattice parameter and elemental composition), improved X-ray analysis using Mo $K\alpha_1$ radiation in combination with density-functional theory calculations reveal a more complicated behavior of the lattice parameter within the entire $Ga_xFe_{4-x}N$ series. The new finding originates from the magnetic properties, and the change in the magnetic ordering with increasing Ga content from ferromagnetic γ'-Fe_4N to antiferromagnetically ordered $GaFe_3N$, as observed from susceptibility measurements, is reproduced by different theoretical spin-alignment models, that is, a systematic evaluation of several antiferromagnetic spin orientations. Nonetheless, all structural models are based on the favored atomic ordering for $GaFe_3N$, explainable by the strong affinity between iron and nitrogen.

Introduction

There are a numerous existing and possible applications for iron nitrides. For instance, γ'-Fe_4N has significant relevance for the mechanical hardening process during steel manufacturing.[1] The combination of its mechanical hardness, its magnetic properties, namely, a large saturation magnetization of 208 emu g^{-1} [2] which is close to that of α-Fe (218 emu g^{-1}), a low coercivity (H_C = 5.8 Oe ≈ 460 A m^{-1})[3] and its high chemical inertness makes γ'-Fe_4N a promising candidate for a high-density recording material.[4−6] Thus, the nitride phase γ'-Fe_4N has been intensively studied by experimental[1,2,7] as well as theoretical investigations.[8,9] The archetypal nitride adopts a perovskite-like structure in space group $Pm\bar{3}m$ (Figure 1).

It is well-known from the literature that the magnetic properties can be tuned and improved with regard to a desired application by substituting the iron atoms on the Wyckoff positions 1*a* and/or 3*c*. Thus, many, mostly berthollide-like, nitrides with the general formula $M_xFe_{4-x}N$ have been described with M = Co,[6] Cu,[10,11] Zn,[12] Ru,[4] Ag,[13] Os[4] and Ir[4] ($x \ll 1$) as well as with Sn ($0 \le x \le 1.2$),[11,14−16] Mn[5] and

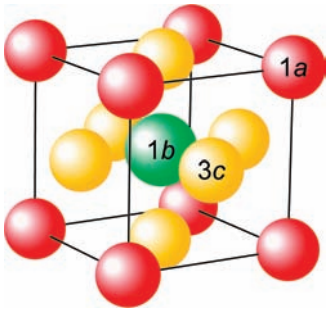

Figure 1. Crystal structure of γ'-Fe_4N in the space group $Pm\bar{3}m$. The green nitrogen atom occupies the very center (Wyckoff position 1*b*). The corner position (Wyckoff position 1*a*) and the face center position (Wyckoff position 3*c*) are occupied by iron. Within $GaFe_3N$, the corner position 1*a* is almost fully occupied by gallium. For interatomic distances, see Table 3.

*To whom correspondence should be addressed. E-mail: drons@HAL9000.ac.rwth-aachen.de. Fax: (+49) 241-80-92642.

(1) Wiener, G. W.; Berger, J. A. *J. Met.* **1955**, *7*, 360.
(2) Chen, S. K.; Jin, S.; Tiefel, T. H.; Hsieh, Y. F.; Gyorgy, E. M.; Johnson, D. W., Jr. *J. Appl. Phys.* **1991**, *70*, 6247.
(3) Guillard, C.; Creveaux, H. *C. R. Hebd. Seances Acad. Sci.* **1846**, *222*, 1170.
(4) Andriamandroso, D.; Matar, S.; Demazeau, G.; Fournès, L. *IEEE Trans. Magn.* **1993**, *29*, 2.
(5) Siberchicot, B.; Matar, S. F.; Fournès, L.; Demazeau, G.; Hagenmüller, P. *J. Solid State Chem.* **1990**, *84*, 10.
(6) Matar, S.; Fournès, L.; ChéRubin-Jeannette, S.; Demazeau, G. *Eur. J. Solid State Inorg. Chem.* **1993**, *30*, 871.
(7) Jacobs, H.; Rechenbach, D.; Zachwieja, U. *J. Alloys Compd.* **1995**, *227*, 10.
(8) Matar, S.; Mohn, P.; Demazeau, G.; Siberchicot, B. *J. Phys.* (*Paris*) **1988**, *49*, 1761.
(9) Kuhnen, C. A.; De Figueiredo, R. S.; Drago, V.; da Silva, E. Z. *J. Magn. Magn. Mater.* **1992**, *111*, 95.
(10) de Figueiredo, R. S.; Foct, J.; dos Santos, A. V.; Kuhnen, C. A. *J. Alloys Compd.* **2001**, *315*, 42.
(11) Stadelmaier, H. H.; Fraker, A. C. *Z. Metallkd.* **1962**, *53*, 48.
(12) Kuhnen, C. A.; de Figueiredo, R. S.; dos Santos, A. V. *J. Magn. Magn. Mater.* **2000**, *219*, 58.
(13) Figueiredo, R. S.; Kuhnen, C. A.; dos Santos, A. V. *J. Magn. Magn. Mater.* **1997**, *173*, 141.
(14) Andriamandroso, D.; Fefilatiev, L.; Demazeau, G.; Fournès, L.; Pouchard, M. *Mater. Res. Bull.* **1984**, *19*, 1187.
(15) Zhao, Z. J.; Xue, D. S.; Li, F. S. *J. Magn. Magn. Mater.* **2001**, *232*, 155.
(16) Zhao, Z. J.; Xue, D. S.; Chen, Z.; Li, F. S. *Phys. Status Solidi A* **1999**, *174*, 249.

Published on Web 10/01/2010

Ni[1,17−19] ($0 \le x \le 4$). The nitrides with M = Ga,[11] Ge[11] ($x \le 1$) and Al[20] are accompanied by other nitridic side-phases incorporating M or iron during synthesis. The iron nitride with Mg[20] has only been briefly mentioned. Furthermore, daltonide phases MFe_3N were obtained with M = Rh,[21,22] Pd,[23] Pt,[1] In,[11,12] and Au.[13]

The first investigation of the iron−gallium−nitrogen system and, in particular, $GaFe_3N$ was published by Stadelmaier and Fraker in 1962.[11] A total of five compositions with different Ga:Fe atomic ratios between 0.3:3 up to 1.3:3 were synthesized using classical NH_3/H_2 ammonolysis reactions at 600 °C. Although no diffractogram had been given, all phases were stated to adopt the crystallographic symmetry of γ'-Fe_4N, namely space group $Pm\bar{3}m$. According to Stadelmaier and Fraker, and independent from the amount of incorporated gallium, all phases were also said to exhibit a lattice parameter of $a = 3.80$ Å which is close to that of γ'-Fe_4N (3.8009(1) Å). With regard to the much larger metallic radius of gallium (r_M(Ga) = 1.41 Å)[24] compared to iron (r_M(Fe) = 1.26 Å),[24] this is a quite unexpected finding, in particular when anticipating a Vegard-like behavior comparable to the analogous ternary iron nitrides of the transition metals.[11,15,17] Nonetheless, considering the covalent radius of gallium (r_{cov}(Ga) = 1.22 Å),[25] which is slightly smaller than for iron (r_{cov}(Fe, l.s.) = 1.32 Å),[25] one might therefore allude to a partially covalent bonding situation. This issue shall be addressed in the theoretical section later on. According to Stadelmaier and Fraker, gallium seems to have a wide solubility range in the binary iron nitride system, despite the fact that all their syntheses were accompanied by the hexagonal side-phase GaN.[26] Unfortunately, the lattice parameters of GaN and the weight fractions were not reported. Up to now, no theoretical investigation of the ternary nitride $GaFe_3N$ has been communicated.

In addition to the aforementioned investigation of the ternary phase $GaFe_3N$, a second study was recently published by us, introducing a phase-pure synthesis by a two-step ammonolysis reaction.[27] In contrast to the former 600 °C synthesis by Stadelmaier and Fraker,[11] a high sintering temperature step (1100 °C, short time) and a subsequent nitridation reaction (530 °C, 3 h) gave access to phase-pure $GaFe_3N$ adopting the typical perovskite-like structure ($Pm\bar{3}m$) with a lattice parameter of $a = 3.7974(1)$ Å, in good agreement with the work by Stadelmaier and Fraker. In the recent study,[27] gallium is exclusively found on Wyckoff position 1*a* with an occupation of about 90%, and in contradiction to the results of Stadelmaier and Fraker a Vegard-type behavior was found for the series of $Ga_xFe_{4-x}N$. Additionally, magnetic measurements using SQUID magnetometry revealed an antiferromagnetic behavior ($\theta_p < 0$ K) of the almost stoichiometric $GaFe_3N$. Increasing the iron amount in exchange for gallium within the $Ga_xFe_{4-x}N$ ($x = 1-0$) system then led to an enlarged magnetic moment measured at a constant external field of $B_0 = 5$ T. This can be explained by a change from an antiferromagnetic to a ferromagnetic behavior upon decreasing the gallium content.

Table 1. Theoretical Absolute Stability of $GaFe_3N$ at Absolute Zero Temperature (0 K) Compared to the Three Most Likely Reactants

reaction	ΔH_R (kJ mol^{-1})
(1) Ga + 3 Fe + 1/2 N_2 → $GaFe_3N$	−87.7
(2) Ga + Fe_3N → $GaFe_3N$	−34.6
(3) GaN + 3 Fe → $GaFe_3N$	+1.8

In the present study, theoretical investigations on the basis of density-functional theory (DFT) were carried out to investigate the thermodynamic stability of $GaFe_3N$. Thus, the total energy of $GaFe_3N$ in comparison to different competing phases was calculated to better understand the nitridation synthesis. Furthermore, a new diffractional technique using Mo $K\alpha_1$ X-ray diffraction (XRD) was employed to shed some new light on the Vegard-like behavior discussed earlier. Additionally, further theoretical investigations were performed to investigate this new behavior and also to explain the magnetic properties of the entire series of compounds. To do so, the structures lowest in energy were investigated such that the most stable atomic configurations and the magnetic properties were predicted and also compared with the experimental findings.

Results and Discussion

At first, we reproduced the phase-pure synthesis of the $Ga_xFe_{4-x}N$ series. To better understand the thermochemistry, the relative stability of $GaFe_3N$ with regard to three possible sets of reactants was calculated (Table 1). It is important to note that, in contrast to the experimental conditions, the starting materials of the theoretical sets of reactants are not the used metal oxides (Ga_2O_3 and Fe_2O_3). Instead, the elements and their nitrides are considered because they are instantly formed through reduction in the hydrogen flow. While these thermochemical calculations are restricted to the ferromagnetic ordering, another magnetic ordering is discussed in the later paragraphs as well.

Table 1 shows three possible reactions with different starting materials giving $GaFe_3N$ as a product. While the first two reactions are exothermic, the third reaction using GaN and iron as reactants is endothermic by about +2 kJ mol^{-1} at absolute zero temperature. To consider finite temperatures, DFT phonon calculations and thermochemical integrations were carried out.[37] These calculations were performed only for the third reaction because of the energies given in Table 1. Because of the inclusion of the zero-point vibrations, the Gibbs free energy for the third reaction GaN + 3 Fe → $GaFe_3N$ is exergonic by about −4 kJ mol^{-1} at zero Kelvin already, and the reaction becomes even more favored with increasing temperature. For the experimentally used reaction temperature of 800 K (530 °C), the Gibbs free energy arrives at about −59 kJ mol^{-1}. Thus, these results are in excellent accordance with the experiment because GaN is only found as a side-phase at lower reaction temperatures.[11] At higher temperatures, a phase pure synthesis results.

Coming back to structural characterization, the large amount of iron in $GaFe_3N$ unavoidably produces a significant

(17) Li, F.; Yang, J.; Xue, D.; Zhou, R. *Appl. Phys. Lett.* **1995**, *66*, 2343.
(18) Rochegude, P.; Foct, J. *Ann. Chim.* **1983**, *8*, 533.
(19) Shirane, G.; Takei, W. J.; Ruby, S. L. *Phys. Rev.* **1962**, *126*, 49.
(20) Stadelmaier, H. H.; Yun, T. S. *Z. Metallkd.* **1961**, *52*, 477.
(21) Houben, A.; Müller, P.; von Appen, J.; Lueken, H.; Niewa, R.; Dronskowski, R. *Angew. Chem., Int. Ed.* **2005**, *44*, 7212.
(22) Houben, A.; Šepelák, V.; Becker, K.-D.; Dronskowski, R. *Chem. Mater.* **2009**, *21*, 784.
(23) Stadelmaier, H. H.; Fraker, A. C. *Transact. Metallurg. Soc. Aime* **1960**, *218*, 571.
(24) Pauling, L. *J. Am. Chem. Soc.* **1947**, *69*, 542.
(25) Cordero, B.; Gómez, V.; Platero-Prats, A. E.; Revés, M.; Echeverria, J.; Cremades, E.; Barragán, F.; Alvarez, S. *Dalton Trans.* **2008**, *21*, 2832.
(26) Juza, R.; Hahn, H. *Z. Anorg. Allg. Chem.* **1938**, *239*, 282.
(27) Houben, A.; Burghaus, J.; Dronskowski, R. *Chem. Mater.* **2009**, *21*, 4332.

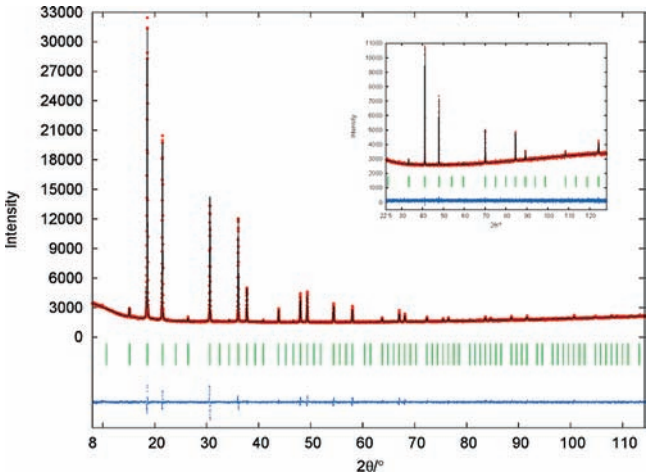

Figure 2. X-ray diffraction pattern and Rietveld refinement plot of $GaFe_3N$ ($Pm\bar{3}m$; a = 3.8001(1)) measured with Mo Kα_1 radiation. The vertical bars designate the positions of the Bragg reflections. The inset shows the diffraction pattern of the same compound but using Cu Kα_1 radiation.

Table 2. Intended Composition x of the $Ga_xFe_{4-x}N$ Series, Refined Lattice Parameter a, Refined Ga Occupation on the 1a Position ${}^{1a}x_{Occ}^{Ga}$, Refined Gaussian-Lorentzian η Mixing Parameters, Related Profile and Bragg Residual Values, Molar Mass M and X-ray Density ρ

x	a (Å)	${}^{1a}x_{Occ}^{Ga}$	η	R_p (%)	R_B (%)	M (g mol^{-1})	ρ (g cm^{-3})
1	3.8001(1)	0.82(6)	0.41	2.25	2.07	251.27	7.60
0.75	3.8000(1)	0.71(5)	0.45	2.60	2.24	247.80	7.50
0.625	3.7978(1)	0.66(6)	0.34	1.81	2.22	246.07	7.46
0.5	3.7962(1)	0.52(6)	0.43	2.26	1.94	244.33	7.42
0.375	3.7964(1)	0.36(5)	0.48	1.99	1.97	246.07	7.47
0.25	3.7968(1)	0.26(6)	0.45	2.18	2.20	240.86	7.31
0.125	3.7975(1)	0.10(6)	0.50	2.06	1.95	239.13	7.25
0	3.8009(1)	—	0.57	2.36	2.56	237.39	7.18

fluorescence background in X-ray diffraction experiments using Cu Kα_1 radiation (λ = 1.54059 Å). Thus, the aforementioned XRD results systematically suffered from an unfortunate intensity-to-background ratio. For this reason, we have now suppressed the fluorescence by using Mo Kα_1 radiation (λ = 0.70932 Å), thereby increasing the overall quality of the X-ray diffraction data. Furthermore, for the same 2θ angular range (8° ≤ 2θ ≤ 130°) the accessible reciprocal space is *much* larger such that the number of reflections is also larger and the statistics are much better. This improvement is obvious when comparing two diffraction patterns, namely, one using Mo Kα_1 radiation and the other using Cu Kα_1 radiation (inset) as illustrated in Figure 2 for $GaFe_3N$ ($Pm\bar{3}m$; a = 3.8001(1) Å).

To complete the whole series, the well-known γ'-Fe_4N was also synthesized in a two-step ammonolysis reaction with a high sintering temperature step (750 °C, 3 h) and a nitridation reaction at 500 °C for 12 h. The results of the Rietveld refinements for all the different compositions are summarized in Table 2 and displayed in Figure 3.

As explained in the last paragraph, the better signal to background ratio (Table 2) is the reason for the smaller experimental standard deviations of the refined gallium occupation on position 1a by using Mo radiation instead to the previous Cu results (see ref 27). As said before, this is explainable by the better statistics and intensity to noise ratio because of the suppressed fluorescence radiation and the larger range of measured d spacings, in particular, since the

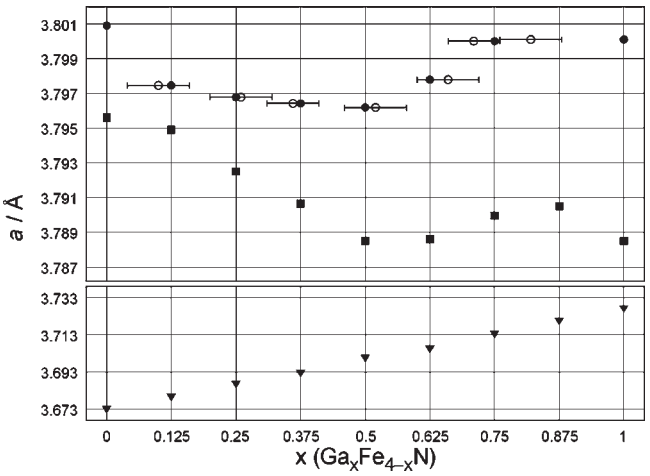

Figure 3. *Top:* Change of the experimental lattice parameters a based on the intended (●), refined (○) and theoretically calculated (■) compositions for the $Ga_xFe_{4-x}N$ series of compounds. The theoretical lattice parameters (■) are based on a ferromagnetic model. The error bars indicate the uncertainty of the occupation on position 1a. With respect to the lattice parameters, their error bars are smaller than the data points themselves. *Bottom:* Change of the lattice parameters a based on a theoretically calculated non-magnetic model (▼).

refinement of the gallium occupation strongly depends on proper intensity values. We also note that the Ga and Fe X-ray form factors are quite close to each other, a true challenge for powder XRD. Nevertheless, the new refinements yield better results in general compared to the preceding ones,[27] and they are also in very good agreement with the ideal composition from the sample preparation.

As shown in Figure 3, γ'-Fe_4N exhibits a lattice parameter of a = 3.8009(1) Å. The substitution of Fe by Ga on 1a leads to a continuous *decrease* of the lattice parameter down to a = 3.7962(1) Å for $Ga_{0.5}Fe_{3.5}N$. With regard to the larger *metallic* radius of gallium (see above), an increase of the lattice parameter should be expected, but considering the smaller *covalent* radius of gallium, a decrease of the lattice parameter is in accordance with experiment and highlights the importance of covalent bonding in this series of compounds. Starting from $Ga_{0.5}Fe_{3.5}N$, the further Ga incorporation then causes a steady *increase* of the lattice parameter up to a = 3.8001(1) Å for $Ga_{0.82}Fe_{3.18}N$, which is the most Ga-rich nitride for this series. For the sake of simplicity, the formula $GaFe_3N$ is used in the further discussion as a replacement of $Ga_{0.82}Fe_{3.18}N$. It is also worth mentioning that the previously determined atomic absorption spectroscopy (AAS) and energy dispersive X-ray (EDX) spectroscopy gave 75(10) and 90(10)% gallium in $GaFe_3N$ under the assumption that gallium exclusively occupies the Wyckoff 1a position as shown by theoretical calculations and Rietveld refinements (XRD) as discussed below.[27] Thus, they are still in good agreement with the newly refined XRD results of 82(6)% Ga occupation on 1a.

To generate the theoretical lattice parameters assuming a ferromagnetic ground state, a supercell was filled, random-like, with different ratios of gallium and iron atoms. In general, all calculated lattice parameters are slightly smaller than the experimental ones, with a maximum deviation of less than 0.3%. The theoretical ferromagnetic lattice parameters do reproduce the non-Vegard-like behavior of the experimental data, in particular with respect to the shrinking volume from γ'-Fe_4N to $Ga_{0.5}Fe_{3.5}N$ but also for the

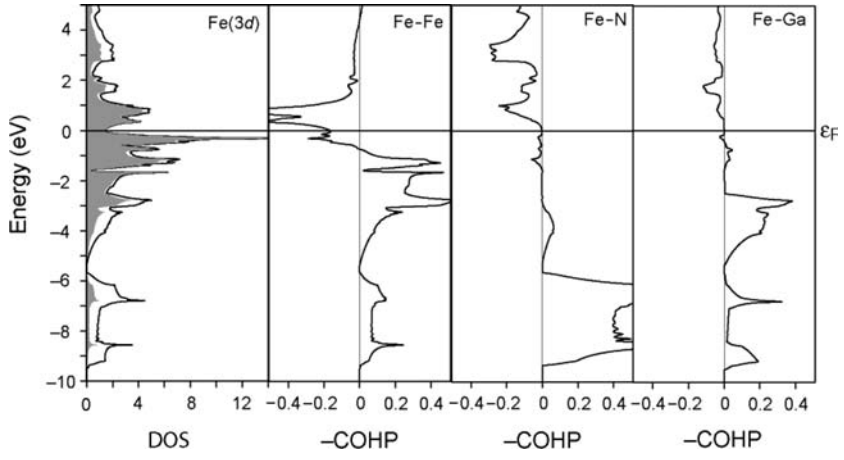

Figure 4. Non-spin polarized DOS and COHP of Fe−Fe, Fe−N, and Fe−Ga interactions within $GaFe_3N$ as obtained from LMTO-GGA calculations. Fe(3d) states are emphasized in gray.

Table 3. Average ICOHP Values from Non-Magnetic LMTO Calculations for Various Interatomic Contacts in $GaFe_3N$ and for Similar Contacts in Related Binary Compounds[a]

	$GaFe_3N$		related compounds			
bond	distance(s) (Å)	ICOHP (eV/bond)		distance(s) (Å)	ICOHP (eV/bond)	$\sum r_{cov}$ (Å)
Fe(3*c*)−Fe(3*c*)	2.687	−0.535	γ'-Fe_4N	2.688	−0.698	2.64
Fe(3*c*)−Ga	2.687	−1.121	Fe_3Ga	2.601	−1.181	2.54
Ga−N	3.291	0.002	GaN	1.949	−1.785	1.93
Fe(3*c*)−N	1.900	−3.705	γ'-Fe_4N	1.900	−3.543	2.03

[a] The sums of the covalent radii r_{cov} are added for comparison.[24] The radius of Fe is the one of the low-spin state.

increasing volume up to $Ga_{0.75}Fe_{3.25}N$; nonetheless, DFT not only overestimates the experimental trend, it also predicts another small decrease of *a* for compositions between $Ga_{0.75}$-$Fe_{3.25}N$ and $GaFe_3N$. Unfortunately, this prediction cannot be checked because of the lack of experimental data. Despite the fact that theory qualitatively reproduces the right trend we doubt that the ferromagnetic model is the optimum choice for $x > 0.5$. [In due course we show that antiferromagnetic $GaFe_3N$ is lower in energy than ferromagnetic $GaFe_3N$. Furthermore, there is a significant difference between the slope of the hysteresis loops for values $x > 0.5$ ($Ga_xFe_{4-x}N$) and $x < 0.5$.[27] Additionally, the hysteretic loops for $x > 0.5$ are not saturated.]

Additionally, a non-magnetic model was used to evaluate the change of the lattice parameter over the whole series of compounds. Figure 3 (bottom) yields much smaller lattice parameters and a Vegard-type like relationship between lattice parameter and composition, in conflict with experiment. Thus, we can safely conclude that the shrinkage/expansion seen before is a *magnetic* effect.

To understand the chemical bonding in $GaFe_3N$, density-of-states (DOS) and various crystal orbital Hamilton population (COHP) curves were calculated. Despite the fact that we deal with a magnetic system, we begin, for reasons of simplicity, with a hypothetically non-magnetic (i.e., non-spin-polarized) calculation (Figure 4) because it already covers much of the chemical bonding trends.

In the total DOS, the Fermi level is located in a pseudogap but still reveals a significant number of states suggesting a metallic character which mostly goes back to the Fe 3d orbitals. With regard to the Fe−Fe interactions, the COHP curve reveals antibonding states at the Fermi level and points toward an electronic instability, namely, the tendency to spin-polarize and become magnetic. The Fe−N and Fe−Ga interactions, on the other side, are nonbonding at the Fermi level. Next to the COHP shapes, the chemical bonding can also be analyzed on the basis of the integrated COHP values (ICOHP) over all occupied levels. The data are given in Table 3 which, for comparison, also includes ICOHP values for similar interactions in related compounds. In general, a larger (more negative) ICOHP value indicates stronger bonding.

Clearly, the major contributors to the structural stability are the Fe−N bonds between −9 and −5 eV, just as expected from chemical intuition. For example, large ICOHP values are found for the Fe(3*c*)−N bond, and the related Fe(3*c*)−N bond in γ'-Fe_4N reveals a comparable (even more bonding, in fact) ICOHP value for the same Fe−N distance. In contrast, the Ga(1*a*)−N interactions in $GaFe_3N$ are evanescent since there is no direct bond, in contrast to hexagonal GaN. In addition, if one numerically compares the Ga−N bond in the binary phase GaN with the Fe−N bond in $GaFe_3N$, the *much* stronger Fe−N interaction mirrors the larger iron−nitrogen affinity and thereby supports the finding that the system energetically favors the occupation of Ga on 1*a* and Fe on 3*c* to yield the stable Fe(3*c*)−N bond. The Fe(3*c*)−Fe(3*c*) distances are slightly longer than the sum of their covalent radii (2.64 Å), and essentially the same Fe(3*c*)−Fe(3*c*) interatomic distances are found in γ'-Fe_4N. Compared to γ'-Fe_4N, the Fe(3*c*)−Fe(3*c*) interactions within $GaFe_3N$ are weaker by 23%, which is compensated by a stronger Fe(3*c*)−N bond within $GaFe_3N$ compared to γ'-Fe_4N (Table 3).

The bonding analysis suggests that the gallium atom exclusively occupies the Wyckoff 1*a* position. To verify this assumption, the atomic ordering was theoretically analyzed

Table 4. Total Energy Differences ΔE (kJ mol^{-1}) between Different Atomic Orderings Relative to an Ordered Occupation ^{1a}(Ga)^{3c}(Fe$_3$)^{1b}(N) and the Corresponding Lattice Parameters a (Å) of GaFe$_3$N in the Perovskite-Like Structure Type[a]

^{1a}(Fe)^{3c}(GaFe$_2$)^{1b}(N)		^{1a}(Ga)^{3c}(Fe$_3$)^{1b}(N)		^{1a}(Ga$_{1/4}$Fe$_{3/4}$)^{3c}-(Ga$_{3/4}$Fe$_{9/4}$)^{1b}(N)	
ΔE (kJmol^{-1})	a (Å)	ΔE (kJmol^{-1})	a (Å)	ΔE (kJmol^{-1})	a (Å)
151	3.87	0	3.79	120	3.87

[a] The calculated data are based on spin-polarized LMTO-GGA calculations.

in more detail because it is the essential basis for understanding the magnetic behavior. At first, the distribution of gallium over the 1*a* and 3*c* positions was analyzed.

The distribution of an ordered phase, namely, ^{1a}(Ga)^{3c}-(Fe$_3$)^{1b}(N) (here, superscripts to the left indicate the Wyckoff position) was compared with another ordered and one statistically disordered phase. The gallium atom can either occupy one-third of the Wyckoff 3*c* positions as given in ^{1a}(Fe)^{3c}(GaFe$_2$)^{1b}(N) or it can be statistically disordered as given in ^{1a}(Ga$_{1/4}$Fe$_{3/4}$)^{3c}(Ga$_{3/4}$Fe$_{9/4}$)^{1b}(N). The energetic results are listed in Table 4.

It is all too obvious that the gallium atom will exclusively occupy the corner position, which is energetically favored by 120 kJ mol^{-1} over the statistical arrangement. This observation is consistent with an independent finding,[28] which relates the atomic ordering to the relative affinity of gallium and iron for nitrogen, verified above, and to the differences in the atomic sizes. The 1*a* site was estimated to correspond to a sphere with a radius of 1.42 Å, whereas the size of the 3*c* site is much smaller (1.28 Å).[4] Only a few ternary iron nitrides, such as the theoretically suggested CoFe$_3$N and the synthesized MnFe$_3$N, are known where M atoms occupy both sites, 1*a* and 3*c* (with $x < 1.0$).[30] Since the covalent radii of cobalt (r_{cov}(Co, l.s.) = 1.26 Å)[25] and manganese (r_{cov}(Mn) = 1.26 Å)[25] as well as the commonly used metallic radii (r_M(Co) = 1.25 Å and r_M(Mn) = 1.26 Å)[24] are smaller than the estimated sphere for the 3*c* site (1.28 Å), an occupation of both sites is energetically preferred. Thus, atoms with a larger radius than 1.28 Å should preferably occupy the 1*a* position. Furthermore, we reiterate that the Fe−N bond is usually the most stable one because of the high iron−nitrogen affinity. For gallium, the very different radii (r_M(Ga) = 1.41 Å[24] and r_{cov}(Ga) = 1.22 Å[25]) render the decision difficult, but both experimental and theoretical results clearly point toward position 1*a* and not 3*c*. Additionally, the calculated lattice parameter (a = 3.79 Å) of the ^{1a}(M)^{3c}(Fe$_3$)^{1b}-(N) model is in excellent agreement with the experimental results (a = 3.8001(1) Å), whereas the two other models both give a lattice parameter of a = 3.87 Å. Thus, we will refer to the ^{1a}(Ga)^{3c}(Fe$_3$)^{1b}(N) ordering in the sequel but note that the theoretical GaFe$_3$N phase is daltonide in contrast to the experimentally synthesized berthollide Ga$_{0.82}$Fe$_{3.18}$N.

Next, we will focus on the magnetic modeling of the Ga$_x$Fe$_{4-x}$N series. As illustrated by the experimental results in Figure 5,[27] an almost linear trend for the magnetic moments going down from 8.96 μ_B (γ'-Fe$_4$N) to 0.87 μ_B (Ga$_{0.82}$Fe$_{3.18}$N) is revealed. In addition, similar measurements of the magnetic saturation moments of Ga$_{0.125}$Fe$_{3.875}$-N (μ_a^s = 7.55 μ_B) and Ga$_{0.375}$Fe$_{3.625}$N (μ_a^s = 5.53 μ_B) were performed at B_0 = ± 5 T that nicely fit into the already published data.[27]

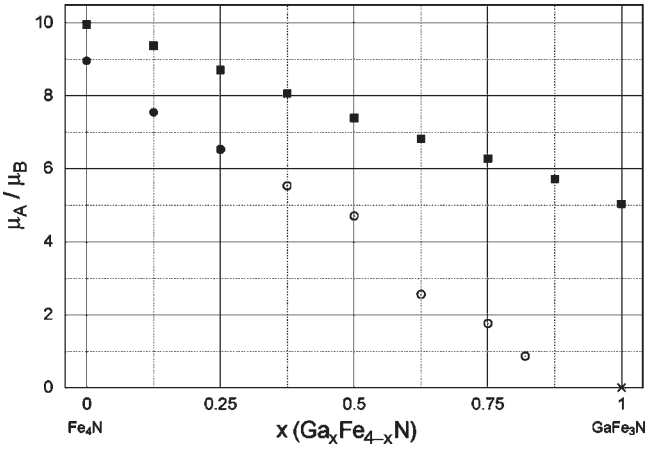

Figure 5. Change of the experimental atomic saturation moments μ_A (●), and experimental unsaturated moments (○) in comparison to the theoretical atomic saturation moments of a ferromagnetic (■) and antiferromagnetic (×) model for the entire Ga$_x$Fe$_{4-x}$N series of compounds.

It is obvious that the experimental magnetic moments decrease from γ'-Fe$_4$N to GaFe$_3$N because iron is substituted by gallium. This trend is correctly reproduced by our theoretical ferromagnetic model that fits well for x = 0.0, 0.125, and 0.25, taking into account that the GGA parametrization by Perdew and Wang[38] usually overestimates such physical properties. For x = 0.375−0.875, however, the theoretical saturation moments are significantly too large than the experimental ones such that the ferromagnetic model must be considered an improper choice. An *antiferromagnetic* model of stoichiometric GaFe$_3$N, however, will converge to a total magnetic saturation moment of zero, and this model will be covered in greater detail below. Finally, both models can at least be used to explain the rapid decrease of the total magnetic moment and the change within the magnetic ordering from the *ferromagnetic* γ'-Fe$_4$N to the *antiferromagnetic* GaFe$_3$N.

With respect to the *antiferromagnetic* ordering, a systematic evaluation of the spin system on the structural basis of different possible arrangements of the Fe spins is needed. Such study needs a larger supercell (Figure 6) which, in our case, consists of eight conventional unit cells. The supercell can be alternatively understood as being composed of four primitive subgrids (Figure 6), namely, one which is gallium-based (black) and three more that are iron-based (red, green and blue). This idea has been adapted from neutron diffraction studies on related perovskite-like structures of the type (La$_{1-x}$Ca$_x$)MnO$_3$ in which different antiferromagnetic arrangements were observed.[29] Within our supercell, elemental gallium is non-magnetic and exclusively occupies the 1*a* position of all eight unit cells, thereby forming the first primitive subgrid of those atoms with the atomic coordinates (0, 0, 0). All iron atoms of the supercell (eight unit cells with three iron atoms each) are discriminated into three subgrids so that each subgrid includes (Figure 6) one of the formerly 3*c* atomic coordinates of a single unit cell, namely, (0, 1/2, 1/2), (1/2, 0, 1/2), and (1/2, 1/2, 0). In the supercell, these iron subgrids were assigned with different primitive spin alignments denoted as A to G (see Figure 6, bottom) to yield an

(28) Cordier-Robert, C.; Foct, J. *Eur. Solid State Inorg. Chem.* **1992**, *29*, 39.
(29) Wollan, E. O.; Koehler, W. C. *Phys. Rev.* **1955**, *100*, 545.
(30) von Appen, J.; Dronskowski, R. *Angew. Chem.* **2005**, *117*, 1230. *Angew. Chem., Int. Ed.* **2005**, *44*, 1205.

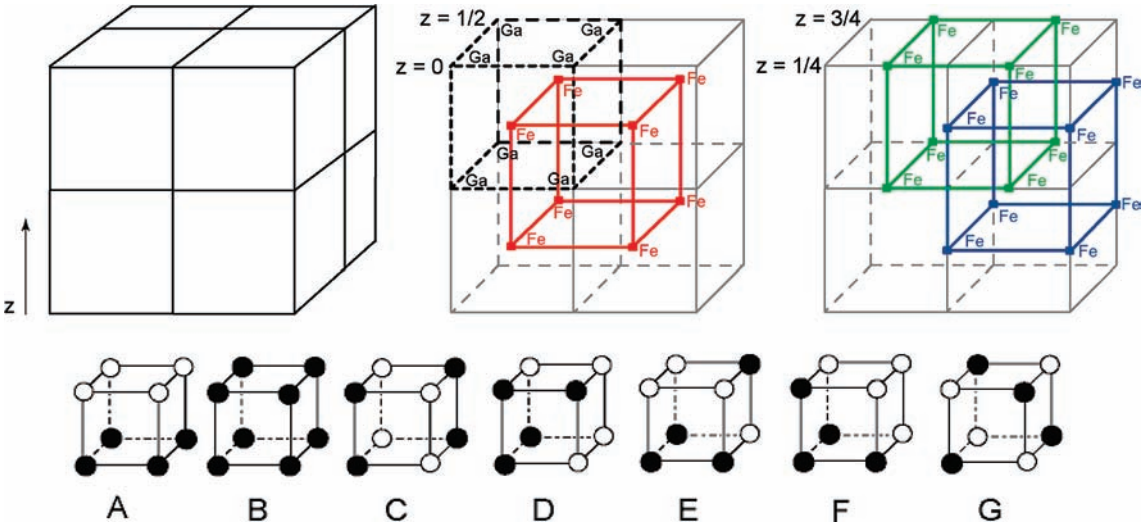

Figure 6. *Top:* Scheme showing the supercell built from eight conventional unit cells (left). Middle and right: Scheme of the four different primitive spin subgrids. One subgrid (in black) is built from eight supercell atoms of the former 1*a* gallium position (0, 0, 0) of the conventional unit cell. The $8 \times 3 = 24$ supercell atoms of the former 3*c* positions yield another three subgrids for each atomic coordinate, namely, composed of red (1/2, 1/2, 0), green (1/2, 0, 1/2), and blue (0, 1/2, 1/2) iron atoms. All the different models of the magnetic orderings can be denoted by a particular subgrid spin arrangement (A−G). *Bottom:* Primitive units cells with different spin arrangements (A−G) in which empty and filled circles relate to opposite spin directions of the Fe atoms.

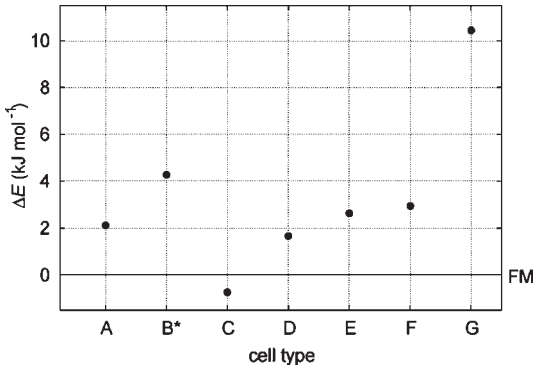

Figure 7. Energetic comparison of different spin arrangements (A−G) compared with the simple ferromagnetic state (FM, horizontal line).

antiferromagnetic supercell. Indeed, such calculations must then converge to a final total magnetic moment of zero for the composition $GaFe_3N$.

We note, however, that the ferromagnetic B-type cell (equal spin-alignment in all subgrids) is in conflict with an antiferromagnetic structure such that one needs to come up with a so-called B*-type cell which is constructed from *two* B-type spin patterns but having *opposite* spin-alignments and one A-type spin pattern to start with an equal number of spin-up and spin-down spins. The energetic results of all the different antiferromagnetic orderings are presented in Figure 7 in comparison to the simple ferromagnetic case which serves as a reference state.

Figure 7 shows that the energy difference between the most unfavorable G-type cell and the energetically most favorable C-type cell is more than 11 kJ mol^{-1}, and the C-type cell is about 1 kJ mol^{-1} more stable than the simple ferromagnetic model (indicated by the energy zero); note, however, that such a small energy difference is even smaller than the accuracy of the DFT method. The C-type cell is characterized by an antiferromagnetic coupling within the *xy* plane and a ferromagnetic coupling along the *z* axis (see Figure 8). The G-type cell, on the other side, exhibits the largest number of antiferromagnetic interactions in all spatial directions (Figure 6), and this leads to the highest-energy structure. "Intermediate" models (e.g., a C-type cell in which a C-spin subgrid is successively substituted by another spin subgrid such as given in the D-type) were also calculated by successive substitution of one cell type by another, but the energetic results were always in-between the results of both aforementioned cell types.

The energetic comparison suggests, first, that the antiferromagnetic ordering is the most stable structure and, second, that a ferromagnetic state is not very far off in terms of energy. Having said that, it is perfectly clear that the ferromagnetic model correctly describes the trend in the decay of the saturation moment with increasing Ga content (Figure 5) but underestimates its size, in particular for large Ga contents where antiferromagnetism really becomes important. Accordingly, Figure 8 shows the DOS and COHP analysis for the lowest-energy antiferromagnetic model of $GaFe_3N$, namely, the C-type cell model.

The DOS plot exhibits the same characteristics as seen before (non-magnetic case, Figure 4). With regard to the C-type antiferromagnetic model we now have to distinguish between antiferromagnetic (AFM) interactions within the *xy* plane and ferromagnetic interactions (FM) along the *z* axis. The antiferromagnetic Fe−Fe interactions (AFM) are plotted in the upper-left COHP while the ferromagnetic (FM) ones are shown in the upper-right COHP. Because of an equal number of majority/minority spins, an exchange splitting can not be seen for the AFM interaction. In contrast, the ferromagnetic bonding reveals the well-known splitting. The minority spin channel (β) has been optimized in terms of bonding, whereas the majority spins (α) occupy small antibonding states at the Fermi level. Nevertheless, the large contributions of antibonding Fe−Fe interactions, as seen within the non-magnetic model (Figure 4) are now annihilated, which translates into an energetic stabilization of the bonding and a stabilization of the whole system. Compared to the non-magnetic model, the Fe−N and Fe−Ga bond (Figure 4) reveal no significant change. On the basis of these results, we verify an

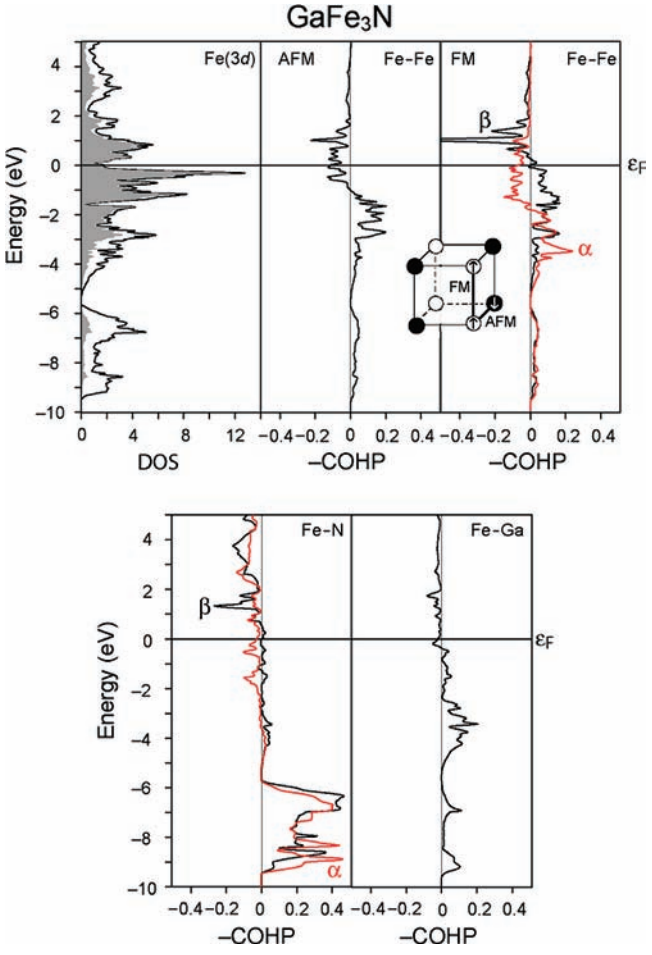

Figure 8. Spin-polarized antiferromagnetic DOS (top, left) and COHP (top, right) of ferromagnetic (FM) and antiferromagnetic (AFM) Fe−Fe interactions as well as the Fe−N (bottom, left) and Fe−Ga (bottom, right) and interactions within the C-type cell $GaFe_3N$ model as obtained from LMTO-GGA calculations.

increased stabilization due to spin polarization. Hence, the preferred magnetic structure is, in accordance to the energetic evaluation, an antiferromagnetic C-type structure.

Conclusion

The reaction between GaN and iron to give $GaFe_3N$ is slightly endothermic (ca. +2 kJ mol^{-1}). DFT phonon calculations and thermochemical integrations, however, yield that the Gibbs free energy for the reaction is exergonic by about −4 kJ mol^{-1} at absolute zero temperature because of the inclusion of the zero-point vibrations, and the reaction becomes even more favored with increasing temperature. For the experimentally used reaction temperature of 800 K (530 °C) the Gibbs free energy is about −59 kJ mol^{-1}. These results are in nice accordance with the experiment because GaN is only found as a side-phase at lower reaction temperatures, while using a higher reaction temperature result in a phase-pure synthesis of $GaFe_3N$.

Improved X-ray analysis using Mo $K\alpha_1$ radiation and theoretical calculations revealed a non-Vegard-like behavior of the lattice parameter as a function of the composition within the $Ga_xFe_{4-x}N$ series. A minimum lattice parameter is found for $Ga_{0.5}Fe_{3.5}N$. The change in the magnetic ordering with increasing gallium content from a ferromagnetic Fe_4N to an antiferromagnetic ordering of $GaFe_3N$ as proposed from macroscopic measurement was reproduced by different theoretical spin alignments.

The theoretical models were based on the favored atomic ordering for $GaFe_3N$, explained by the strong affinity between iron and nitrogen, since the formation of the Fe(3*c*)−N is significantly stabilized compared to a Ga−N bond. Therefore gallium occupies only position 1*a*, whereas iron goes on position 3*c*. We have suggested several spin alignments for the antiferromagnetic compound $GaFe_3N$, but neutron diffraction studies have to be carried out to corroborate the magnetic structures.

Experimental Section

Synthesis of $Ga_xFe_{4-x}N$.[27] The powdered reactants Ga_2O_3 and Fe_2O_3 were mixed and accurately ground using the desired ratio of the metal atoms. For the optimized synthesis a two-step ammonolysis reaction with a high sintering temperature step (1100 °C, 1 min) and a nitridation reaction (530 °C, 3 h) gave access to phase-pure $GaFe_3N$. The ammonolysis gas was a NH_3:H_2 mixture with a 1:1 ratio.

Computational Details. Theoretical determination of the structural and electronic properties were carried out using the Vienna ab initio simulation package (VASP),[31−33] based on DFT using plane-wave basis sets. Projector-augmented-wave (PAW) potentials were used,[34,35] describing the exchange-correlation potential with the generalized gradient approximation (GGA) parametrized by Perdew and Wang.[38] An 8 × 8 × 8 Monkhorst−Pack[39] *k*-point grid for one supercell containing eight formula units was used for integrations within the Brillouin zone. Spin-polarized calculations for the ferromagnetic case were performed with integer starting values for all local magnetic moments, namely, 3 for all magnetically active elements and 0 for all other elements. Forces, stress tensors, atomic positions, unit cell shapes, and unit cell volumes of the crystal structures were allowed to relax during optimization. Because of the expected small energy differences, the convergence criterion of the electronic structure calculation was set to 0.01 meV. Theoretical phonon data were calculated using the quasi-harmonic approximation by means of the FROPHO utility[36] together with VASP, and thermodynamical state functions were then generated using a set of script programs[37] on the basis of the density-functional electronic structure. Chemical bonding analyses on the lowest-energy structures elucidated from VASP calculations were performed on the basis of first-principles electronic band structures and magnetic moments calculated with the Tight-Binding Linear Muffin-Tin Orbital (TB-LMTO) method[40] by employing the nonlocal generalized gradient approximation (GGA) for exchange and correlation. The specific method used was Linear Muffin-Tin Orbital theory[41] which represents a fast, linearized form of the KKR method.[42,43] The TB-LMTO calculations were carried out within the Atomic Spheres Approximation (ASA).[40,41] No empty spheres were

(31) Liu, S. *Phys. Rev. B* **1977**, *15*, 4281.
(32) Kresse, G.; Furthmüller, J. *Comput. Mater. Sci.* **1996**, *6*, 15.
(33) Kresse, G.; Hafner, J. *Phys. Rev. B* **1993**, *47*, 558.
(34) Blöchl, P. E. *Phys. Rev. B* **1994**, *50*, 17953.
(35) Kresse, G.; Joubert, J. *Phys. Rev. B* **1999**, *59*, 1758.
(36) Togo, A.; Oba, F.; Tanaka, I. *Phys. Rev. B* **2008**, *78*, 13410.
(37) Stoffel, R. P.; Wessel, C.; Lumey, M. W.; Dronskowski, R. *Angew. Chem., Int. Ed.* **2010**, *49*, 5242.
(38) Perdew, J. P.; Wang, Y. *Phys. Rev. B* **1992**, *45*, 13244.
(39) Monkhorst, H. J.; Pack, J. D. *Phys. Rev. B* **1976**, *13*, 5188.
(40) Andersen, O. K.; Jepsen, O. *Phys. Rev. Lett.* **1984**, *53*, 2571.
(41) Andersen, O. K. *Phys. Rev. B* **1975**, *12*, 3060.
(42) Korringa, J. *Physica* **1947**, *13*, 392.
(43) Kohn, W.; Rostoker, N. *Phys. Rev.* **1954**, *94*, 1111.
(44) Krier, G.; Jepsen, O.; Burkhardt, A.; Andersen, O. K. *TB-LMTO-ASA*, V4.7c; Max-Planck-Institut für Festkörperforschung: Stuttgart, Germany.

necessary to achieve space filling. The Perdew−Wang nonlocal exchange correlation potential as implemented in the LMTO code[44] was used for the GGA calculations. A total of 64 up to 455 irreducible *k*-points were needed for Brillouin zone integrations using the tetrahedron method.[45] Self-consistency was achieved when the total energy change was smaller than 0.01 mRy (0.136 meV). The chemical bonding analyses were based on the density of states (DOS) and crystal orbital Hamilton population (COHP) curves.[46]

XRD and Rietveld refinement. X-ray diffraction at room temperature for $Ga_xFe_{4-x}N$ was performed using a calibrated STADI MP (STOE Darmstadt) powder diffractometer with Mo $K\alpha_1$ radiation ($\lambda = 0.709320$ Å; flat sample; $8 \leq 2\theta \leq 130°$, step rate 0.01° in 2θ). The Rietveld refinement was carried out with the program FullProf[47] and a pseudo-Voigt profile function. The refinement parameters and the residual values for the series of $Ga_xFe_{4-x}N$ are listed in Table 2. The positions are 1*a* for Ga, 1*b* for N, and 3*c*/1*a* for Fe within space group $Pm\bar{3}m$. By constraining the sum of the occupation parameters of iron and gallium on 1*a* to unity, the gallium contribution for this position can be refined. Likewise, the iron occupation on position 3*c* was refined to be 100%.

SQUID. Hysteresis loops were recorded at a temperature of 5 K in the field range ±5 T by SQUID magnetometry (MPMS-5S, Quantum Design).

Acknowledgment. It is a pleasure to thank Dr. Paul Müller for having performed X-ray measurements, Dr. M. Speldrich for the SQUID measurements, and Deutsche Forschungsgemeinschaft for having funded this study. We thank the computing center of RWTH Aachen University for providing us with their supercomputing facilities.

(45) Blöchl, P.; Andersen, O. K.; Jepsen, O. *Phys. Rev. B* **1994**, *34*, 16223.
(46) Dronskowski, R.; Blöchl, P. E. *J. Phys. Chem.* **1993**, *97*, 8617.
(47) Rodriguez-Carvajal, J. *FULLPROF*, Version 4.0; May 2007, ILL (unpublished).